

Effect of Stacking Order on the Electronic State of 1T-TaS₂

Zongxiu Wu,¹ Kunliang Bu,¹ Wenhao Zhang,¹ Ying Fei,¹ Yuan Zheng,¹
Jingjing Gao,^{2,3} Xuan Luo,² Zheng Liu,⁴ Yu-Ping Sun,^{2,5,6} and Yi Yin^{1,6,*}

¹*Zhejiang Province Key Laboratory of Quantum Technology and Device,
Department of Physics, Zhejiang University, Hangzhou 310027, China*

²*Key Laboratory of Materials Physics, Institute of Solid State Physics,
Chinese Academy of Sciences, Hefei 230031, China*

³*University of Science and Technology of China, Hefei 230026, China*

⁴*Institute for Advanced Study, Tsinghua University, Beijing 100084, China*

⁵*High Magnetic Field Laboratory, Chinese Academy of Sciences, Hefei 230031, China*

⁶*Collaborative Innovation Center of Advanced Microstructures, Nanjing University, Nanjing 210093, China*

New theoretical proposals and experimental findings on transition metal dichalcogenide 1T-TaS₂ have revived interests in understanding the origin of the strongly correlated insulating state. The coexistence and competition of charge density wave, electron-electron interaction, and interlayer hopping make the problem challenging. We perform comprehensive scanning tunneling microscopy and spectroscopy measurements on different single-step areas in pristine 1T-TaS₂. After accurately determining the relative displacement of Star-of-David super-lattices on two layers, we find different stacking orders corresponding to the electronic state's discrepancy on the surface. The center-to-center stacking corresponds to the universal large gap, while other stacking orders correspond to a reduced or suppressed gap in the electronic spectrum. Adopting a unified model, we conclude that the universal large gap is a Mott gap derived from single layer property. Our work provides more evidence about the surface electronic state and deepens our understanding of the Mott insulating state's nature in 1T-TaS₂.

I. INTRODUCTION

Mott insulator is a vital quantum phase of the strongly correlated system [1, 2]. Due to the strong correlation between electrons, a half-filled metallic band can be split into a lower and upper Hubbard band (LHB and UHB) with a middle insulating gap [2–5]. The parent compound of High- T_c cuprate superconductors (HTS) is a typical Mott insulator [6, 7]. In fact, the strong interest in Mott insulators stems from the desire to clarify the underlying mechanism of HTS. After decades of research on HTS, finding other Mott insulators and studying their insulator-metal transition has become a new intriguing field [8–11].

Layered transition metal dichalcogenide (TMD) 1T-TaS₂ is widely considered to host a correlation-induced Mott insulating phase [12–14]. A special property of 1T-TaS₂ is that it enters a series of charge-density-wave (CDW) phases after the temperature is lowered [4, 5, 12, 15, 16]. Below around 170 K, the material is at a commensurate CDW (CCDW) state with a $\sqrt{13} \times \sqrt{13}$ reconstruction [Fig. 1(a)], which in turn leads to a metal-insulator transition. On one hand, the multi-folded band of super-lattice induces a flat band around the Fermi energy, whose narrow bandwidth allows a general correlation strength to be classified as a strong correlation limit. On the other hand, the electronic state is more susceptible to external perturbations, making the Mott insulating state of pristine 1T-TaS₂ easy to be modulated [12, 17–24].

The super cell of the CCDW phase consists of 13 Ta atoms with 12 surrounding Ta atoms slightly shrinking to the central Ta atom [Fig. 1(a)], commonly referred to as the Star of David (SD). The super-lattice constant between two SDs is around 12 Å, several times longer than the lattice constant and the interlayer spacing (~ 5.9 Å). Although stacked layers of 1T-TaS₂ are bonded by a weak Van der Waals interaction, the role of interlayer coupling in electronic structure is always a controversial problem due to the large ratio between the super-lattice constant and the interlayer spacing.

Scanning tunneling microscopy (STM) is a microscopic technique to detect the local electronic density of states (DOS) of materials. Typically, pristine 1T-TaS₂ shows a Mott insulating gap around the Fermi level [23–27]. A mosaic metallic state was induced by a tip-induced voltage pulse in 1T-TaS₂, which reflects that altered interlayer stacking orders can result in either a Mott insulating or metallic state [23, 24]. Recently two different insulating spectra were found under altered interlayer stacking orders, suggesting that the stacking order can modulate the electronic state in some way [28]. Puzzlingly, the insulating gap found in the single layer 1T-TaS₂ grown by molecular beam epitaxy (MBE) appears very similar to that observed on the bulk surface [29]. Relevantly, a correlated Mott insulator was identified in a cousin material of single layer 1T-TaSe₂ [30, 31], although the bulk 1T-TaSe₂ is a metallic material [32]. First-principles calculations indeed revealed significant band renormalization induced by the interlayer coupling [33, 34]. However, it is still challenging to simulate the realistic interlayer staking patterns. At the present stage, a systematic and comprehensive understanding is still lacking on the effect

* yiyin@zju.edu.cn

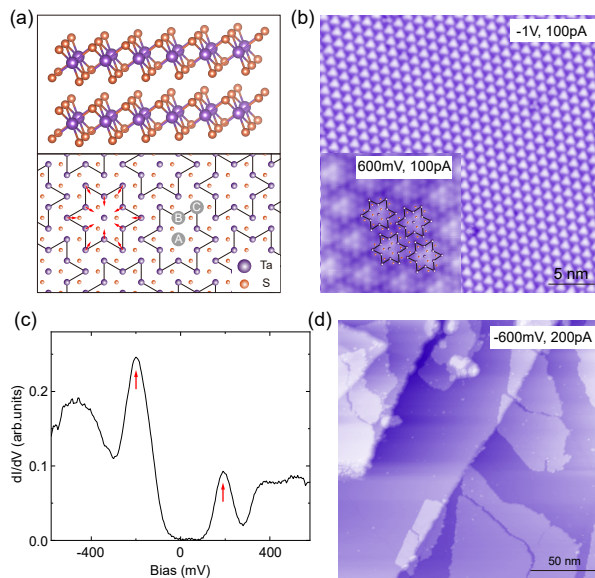


FIG. 1. **Structural and electronic properties of 1T-TaS₂.** (a) The upper panel shows the atomic structure of 1T-TaS₂. The lower panel is a top-view diagram, with the purple and yellow balls representing the Ta atoms and the uppermost S atoms, respectively. Ta atoms can be divided into central, inner-corner, and outer-corner sites, which are labeled by A, B, and C, respectively. The red arrow indicates the shrinking of the surrounding 12 Ta atoms toward the central Ta. (b) A typical 30 × 30 nm² topography in a flat area. The inset displays an atomic resolved topography under the tunneling condition of $V_b = 600$ mV, $I = 100$ pA. (c) The typical insulating dI/dV spectrum of 1T-TaS₂. The red arrows label the upper and lower Hubbard bands. (d) A complex surface topography.

of stacking order.

Here in this work, we report precise STM determinations of various interlayer alignments and the associated electronic spectra by purposely creating and exploring single-step areas of the cleaved 1T-TaS₂. We find that when the SD centers of the top and underlying layers coincide (AA stacking), the dI/dV spectra of both layers display a ~ 400 meV gap, similar to that observed in a single-layer MBE sample [29]. When the SD centers do not coincide, the dI/dV spectrum of the top layer displays varying features, such as a much smaller insulating gap or even an insulator-metal transition. These observations cannot be naturally explained by a simple interlayer dimerization mechanism [28]. We propose that interlayer misalignment plays an important role in modulating the electronic structure of a single TaS₂ layer, and the interlayer effect is minimal under a perfect AA stacking order.

II. EXPERIMENT AND RESULTS

Each layer of 1T-TaS₂ is comprised of a triangular lattice of Ta atoms sandwiched between the top and bottom

triangular lattice of S atoms. Each Ta atom is coordinated octahedrally by S atoms. In the CCDW phase, each SD cluster is formed by 13 Ta atoms, classified by one central Ta atom (position A), six neighboring Ta atoms at inner-corner site (position B), and six next neighboring Ta atoms at outer-corner site [position C in Fig. 1(a)]. In our previous work [16], we found that a substrate with different thermal expansion coefficient than the sample can induce local strain and change the surface appearance. Here we glue the sample on a silica substrate, and cleave the sample at liquid nitrogen (LN₂) temperature. This treatment is found relatively easy to create a surface topography with multiple steps as shown in Fig. 1(d). In comparison, gluing the sample on the commonly used beryllium copper sheet results in a flat surface as shown in Fig. 1(b)]. The cleaved sample is thereafter quickly transferred to the STM scan head in the cryogenic Dewar. We also perform the following STM measurement at LN₂ temperature.

The SD super-lattice can be most clearly resolved from the flat surface topography [Fig. 1(b)], with each bright spot representing one SD. When the tip is occasionally under special conditions, the surface exposed S atoms can be atomically resolved within SDs [inset of Fig. 1(b)]. A typical dI/dV spectrum measured at one SD center is shown in Fig. 1(c). The two coherence peaks roughly at ± 200 mV correspond to the upper and lower Hubbard bands (UHB and LHB), with an insulating gap of 400 meV. Peaks outside the Hubbard bands are related with CDW features.

The flat single-step area renders a determination of the relative displacement of SD super-lattices on the upper and lower terrace. Multiple measurements have been collected for different samples with different tips. Figure 2(a) shows the topography of the first example of a single-step area. The bright region is a smooth top layer of 1T-TaS₂, with the purple region the smooth underlying layer. For both top and underlying layers, the topography includes a triangular SD super-lattice and each bright spot represents one SD. Figure 2(b) shows two dI/dV spectra measured on the lower and upper terrace, respectively. Both spectra are similar to the spectrum in Fig. 1(c). To check how the electronic state evolves from the upper terrace to the lower terrace, a linecut map is measured along the arrowed line in Fig. 2(a). In Fig. 2(c), the horizontal axis is the position along the arrowed line, the height profile in the bottom panel shows a rising single step in the middle, and the linecut map of dI/dV spectrum in the top panel shows a periodic intensity variation on both the lower and upper terrace. Modified spectra around the step edge go beyond the content of this paper.

With both the upper and lower terrace exposed, we can analyze the relative shift between the top and bottom super-lattices. We choose a rectangular area, four corners of which are on the bottom layer while the peninsula is enclosed within the chosen area. Around each corner, several SD centers are positioned with a peak-seeking al-

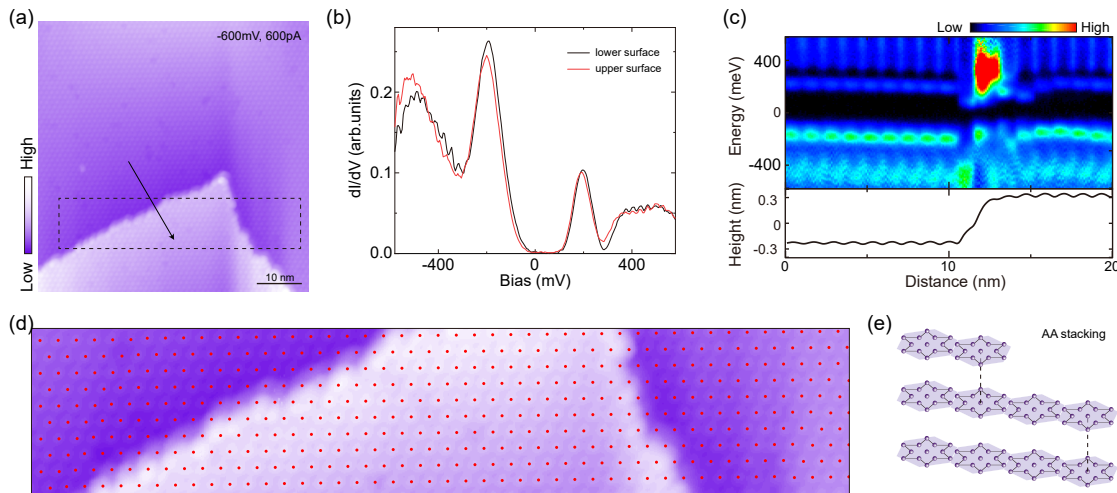


FIG. 2. **AA-type stacking single-step area with a large-gap spectrum.** (a) The STM topography of the single-step area. (b) The red and black curves show the dI/dV spectra on the upper and lower terrace, respectively. Both spectra are similar to the typical dI/dV spectrum in Fig. 1(c). (c) A series of dI/dV spectra measured along the black arrowed line in (a), with the height profile displayed in the lower panel. (d) The determination of SD super-lattice for area in the black dashed frame in (a). (e) A schematic diagram of the AA-type stacking order.

gorithm. With anchored positions between different corners, a linear fitting leads to a SD array for the lower terrace, as shown by the red dots in Fig. 2(d). The positioning accuracy can be confirmed by comparing the dot position with the SD in topography, for the exposed part of lower terrace. We can further observe that red dots at the peninsula coverage area coincides with the SD centers in upper terrace. The SD centers of upper and lower terrace are aligned in the c -axis direction. This stacking order can be defined as the AA-type stacking [Fig. 2(e)].

For the second example of a single-step area, the topography is shown in Fig. 3(a). The red dashed line on the upper terrace marks a domain wall, with the SD super-lattices in two domains have a translational shift, or phase shift to each other. At locations of three points marked in the image, the dI/dV spectra are measured on the lower terrace, and two domains of upper terrace, respectively. As shown in Fig. 3(b), the spectrum on the lower terrace is still an insulating spectrum similar to the one in Fig. 1(c). In contrast, the spectra on both domains in upper terrace are different. The UHB and LHB peaks appear to be shifted to 140 and -100 mV, and the LHB also contains another lower energy peak at -205 mV. Following we call the two types of spectra a large-gap spectrum and a small-gap spectrum, respectively. A linecut map is also measured along the arrowed line in Fig. 3(a). A rising single step is shown in the height profile. The modified spectra around the step edge and domain wall position also go beyond discussion in this paper. From the periodic intensity variation of dI/dV spectrum on the upper terrace, we can observe that the three shifted peaks around Fermi energy (zero bias) are still evident at the SD centers, representing that they are from the Hubbard bands of central Ta orbital [25].

To study the stacking order of upper and lower ter-

race, we need to position the SD centers in the three regions around the peninsula area. A similar method as in the first example is applied to extract a SD array for the lower terrace, as shown by the red dots in Fig. 3(d). The difference here is that, the SD centers of upper terrace, labeled by blue and green dots for two domains, are observed to be not aligned with that of lower terrace. Due to the lattice symmetry in $1T$ -TaS₂, positioning of SD centers corresponds to two possible atomic arrangements, which differ with a 27.8° rotation of each SD. We further apply a specific point defect to obtain the only definite atomic lattice, with the method shown in Appendix A. Correspondingly, both the SD centers and the SD arrangement of lower terrace are superimposed on the enlarged topographies in Fig. 3(e) and 3(f). We can observe that the SD centers on upper terrace are aligned with the next nearest Ta atoms in each SD on lower terrace. This stacking order can be defined as the AC-type stacking [Fig. 3(g)].

For the third example of a single-step area, the topography is shown in Fig. 4(a). Figure 4(b) shows two dI/dV spectra measured on the lower and upper terrace, respectively. The spectrum on the lower terrace is a large-gap insulating spectrum. The spectrum on the upper terrace is very different, with the zero-bias conductance strongly enhanced, later called a metallic spectrum. From the linecut map measured along the arrowed line [Fig. 4(c)], we obtain how the spectrum evolves from a large-gap insulating spectrum to a metallic spectrum. From the periodic intensity variation, we also observe that the coherent peaks of metallic spectrum are evident at the SD centers and originate from the Hubbard bands of central Ta orbital [25].

The SD centers in the upper and lower terrace are similarly determined as above. A SD array is obtained for the

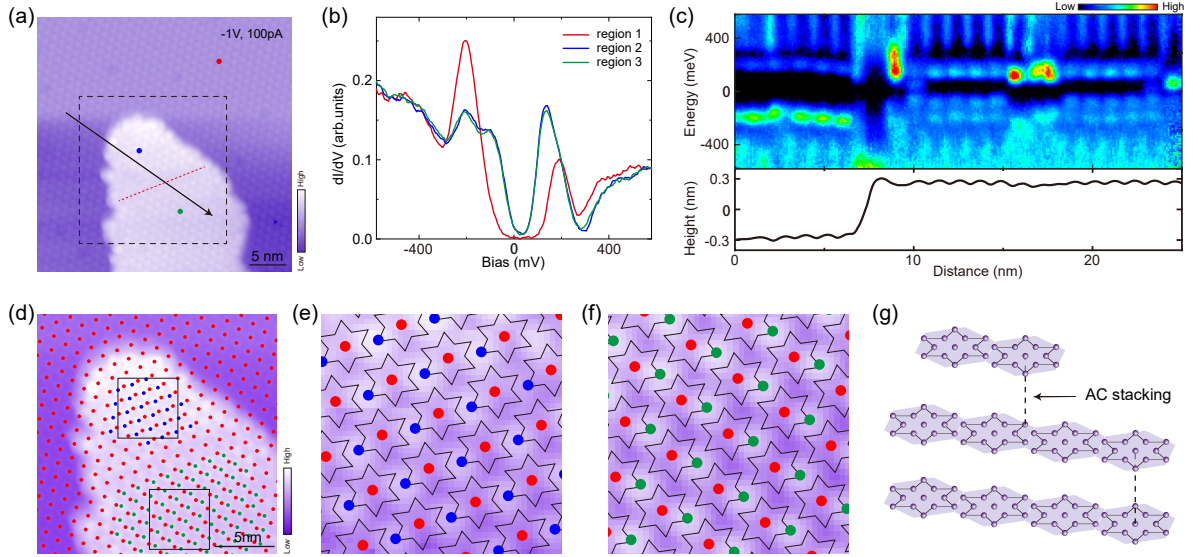


FIG. 3. AC-type stacking single-step area with a small-gap spectrum. (a) The STM topography of the single-step area. The red dashed line indicates a domain wall on the top terrace. (b) The three dI/dV curves correspond to the electronic states measured at the red, blue, and green dot positions in (a), respectively. The spectrum on the lower terrace is the typical insulating spectrum, and the spectrum on both sides of the domain wall on the upper terrace is one with a smaller gap. (c) A series of dI/dV spectra measured along the black arrowed line in (a), with the height profile displayed in the lower panel. (d) The determination of SD super-lattices for the area in the black dashed frame in (a). The red dots label SD centers on the lower terrace, and the blue and green dots label SD centers on both sides of the domain wall on the upper terrace. (e), (f) The enlargement of the two black boxes in (d). The SD centers on both sides of the domain wall are aligned with the SD outer-corner sites in lower terrace. (g) A schematic diagram of the AC-type stacking order.

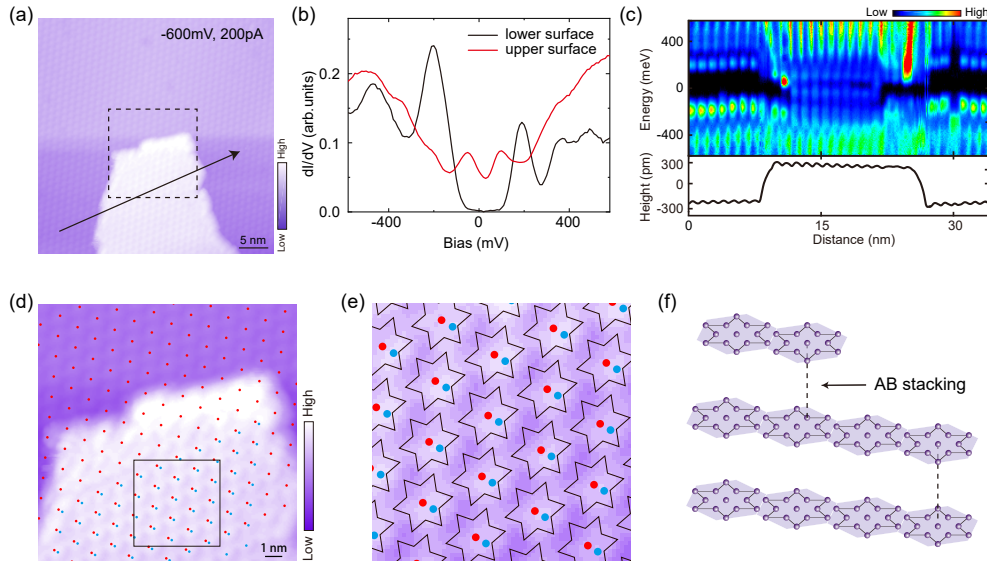


FIG. 4. AB-type stacking single-step area with a metallic spectrum. (a) The STM topography of the single-step area. (b) The red and black curves show the dI/dV spectra on the upper and lower terrace, respectively. The spectrum on the lower terrace is also the typical insulating spectrum, and on the upper terrace is a metallic spectrum. (c) A series of dI/dV spectra measured along the black arrowed line in (a), with the height profile displayed in the lower panel. (d) The determination of SD super-lattices for the area in the black dashed frame in (a). The red dots label SD centers of the lower terrace, and the blue dots label SD centers in the upper terrace. (e) The enlargement of the black box in (d). The SD centers on the upper terrace are aligned with the SD inner-corner sites in lower terrace. (f) A schematic diagram of the AB-type stacking order.

lower terrace, as shown by the red dots in Fig. 4(d). The blue dots represent a shifted SD array compatible with the SD lattice of upper terrace [Fig. 4(d)]. In Fig. 4(e), both the SD centers and the SD arrangement of lower terrace are superimposed on the enlarged topography. We can observe that the SD centers on upper terrace are aligned with the nearest Ta atoms in each SD on lower terrace. This stacking order can be defined as the AB-type stacking [Fig. 4(f)].

During the measurement of single-step areas, we find that the above correspondence between stacking orders and electronic states are constantly reproducible. For above three examples, the first two are the most common cases. The large-gap spectrum can extend all the way in from the step edge. On the contrary, the small-gap spectrum often presents within a certain range of the step edge, e.g. 20 nm. We conclude that the dI/dV spectrum measured on an exposed surface is a large-gap spectrum when this layer is AA-stacked with underlying layer, is a small-gap spectrum when the layer is AC-stacked with underlying layer, or is a metallic spectrum when the layer is AB-stacked with underlying layer. Because the dI/dV measured on the lower terrace is always a large-gap spectrum, we assume that the lower terrace is also AA-stacked with the unexposed layer below, as depicted in Fig. 2(e), Fig. 3(e), and Fig. 4(f). The AA-stacking seems to be an energy optimal situation in the bulk material. The normal flat surface is AA-stacked with underlying layer, resulting in a large-gap insulating spectrum. Sometimes the AC-stacking occurs around edges of the terraced region.

The coexistence of two large-gap spectra on both upper and lower terrace in the first example rules out the possibility that the large-gap spectrum originates from a unit-cell doubling of two neighboring layers. A more reasonable model is that the large-gap spectrum is consistent with the single layer property, like that measured on the single layer MBE grown film of $1T$ -TaS₂. When one layer is AC-stacked or AB-stacked with the underlying layer, the stacking order delicately affects spectrum on the top layer, resulting in a small-gap spectrum or a metallic spectrum, respectively. Please note that we can only measure and determine the electronic state on exposed terraced areas.

In the process of collecting and analysing data, we also find some uncommon examples as shown below. Figure 5(a) is a topography around a single-step area, on which the SD centers on both upper (blue dots) and lower (red dots) terrace are superimposed. From the SD arrangement of the lower terrace, we can observe that the SD centers on the upper terrace are aligned with the SD outer-corner sites in lower terrace. We further determine that this case is under an AC'-stacking. The AC'-stacking is different from the normal AC-stacking, where the SD center in one layer is vertically aligned with the unequivalent outer-corner of SDs in the underlying layer [Fig. 5(c)]. Figure 5(b) shows two dI/dV spectra measured on the lower and upper terrace, respectively.

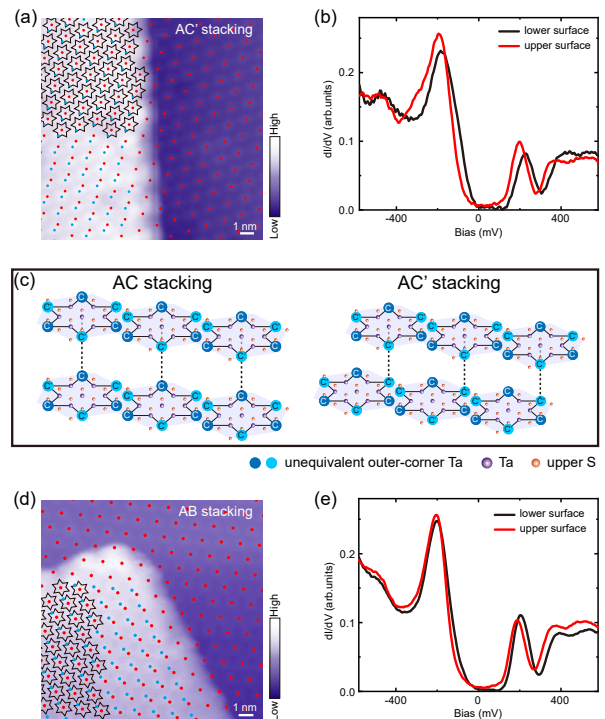


FIG. 5. Two uncommon examples on the single-step area. (a) The STM topography of one single-step area. The red (blue) dots label SD centers of the lower (upper) terrace. The SD centers on the upper terrace are aligned with an unequivalent SD outer-corner sites in lower terrace, or in the AC'-type stacking order. (b) The red and black curves show the dI/dV spectra on the upper and lower terrace in (a), respectively. (c) Schematic diagrams of the AC-type stacking order and AC'-stacking order. (d) The STM topography of another single-step area, which is in the AB-type stacking order. (e) The red and black curves show the dI/dV spectra on the upper and lower terrace in (d), respectively.

The anomalous result is that both spectra are similar to the large-gap spectrum. Figure 5(d) shows a topography with an AB-type stacking. The anomalous dI/dV spectra in Fig. 5(e) are also two large-gap spectra. In both examples, the zero-bias conductance of the upper-terrace spectrum is slightly enhanced.

The same stacking order can lead to different results suggests that other factors may have played a role. We also do not exclude that other uncommon cases could occur. These two examples further exclude that the large-gap spectrum originates from a unit-cell doubling of two neighboring layers. In such cases, the upper-terrace spectrum is not strongly altered in the AC'-stacking or AB-stacking conditions, or the single-layer large-gap spectrum is well maintained. The slight enhancement of zero-bias conductance may reflect a weak modulation. We notice that the large-gap spectrum has been previously found in an AC'-type stacking in a metastable system induced by voltage pulses [24]. Our results are all in a stable state. In addition, we never observe the AA-type stacking together with a small-gap or metallic spectrum,

which is consistent with that the AA-type stacking minimally affects the single-layer large-gap spectrum.

III. CONCLUSION

The three stacking patterns were also studied in [28]. We note that all the typical spectra shown in [28] are also observed in our sample, but a key difference is that we show for AA stacking the large-gap spectra does not necessarily change across the step. This largely rules out a simple AA-AC-AA-AC alternating stacking order in our sample. Therefore, it is clear that the large insulating gap is not associated to AA dimerization, which can actually be well compared with that observed in a MBE single-layer TaS₂ [29].

In conclusion, our experimental results show that the Mott gap of a single TaS₂ layer is nearly unperturbed under AA stacking, while the interlayer misalignment tends to destroy the Mott gap. A possible explanation is that the misalignment weakens the CCDW amplitude, on which the Mott physics sensitively relies. Further theoretical investigations are required to clarify the subtle interplay between electron correlation, CDW and inter-layer coupling.

ACKNOWLEDGMENTS

This work was supported by the National Key Research and Development Program of China (Grants No. 2019YFA0308602), the Key Research and Development Program of Zhejiang Province, China (2021C01002), and the Fundamental Research Funds for the Central Universities in China. Z.L. thanks the National Nature Science Foundation of China (NSFC-11774196) and Tsinghua University Initiative Scientific Research Program. J.J.G., X.L., and Y.P.S. thank the support of the National Key Research and Development Program of China (Grants No. 2016YFA0300404), the National Nature Sci-

ence Foundation of China (NSFC-11674326 and NSFC-11874357), the Joint Funds of the National Natural Science Foundation of China, and the Chinese Academy of Sciences' Large-Scale Scientific Facility (U1832141, U1932217, U2032215).

Appendix A: A Special Type of Point Defect in 1T-TaS₂

Figure 6 shows representative data for a particular type of defect we find in 1T-TaS₂. Figure 6(a) and 6(b) are two topographic images taken at the same area with bias voltage at 600 mV and -1000 mV, respectively. A three-petal shaped defect can be observed in the middle of both images, pointing in the same direction but with the three petals in Fig. 6(b) gathered closer. We notice that each star of David (SD) is a triangle in the topography, with the direction of triangle in both topographies inverted. Figure 6(c) shows two dI/dV spectra measured at the center of the three-petal defect and a normal SD. Compared with the normal large-gap spectrum, the defect spectrum shows a totally suppressed UHB while the LHB is left with a raised peak at -300 mV.

Occasionally the atomic resolved topography can be obtained when the tip is under a special condition. Figure 6(d) and 6(e) are two topographic images at the same area, with Fig. 6(d) showing the atomic-resolved surface, on which the top S atoms can be discerned. The brightest atoms in each SD are the three nearest neighboring S atoms of the central Ta, leading to the triangle SDs in Fig. 6(e). The dashed triangles in Fig. 6(d) and 6(e) directly illustrate that the three-petal feature of the defect corresponds to the sites of next nearest S atoms of the central Ta atom. In Fig. 6(d), the black hole within the defect area indicates that the defect is possibly a missing central Ta, with both UHB and LHB suppressed in the defect spectrum. The origin of the raised peak below LHB is still an open question at current status. Then this special type of point defect can help to determine the atomic lattice arrangement as shown in Fig. 6(f).

-
- [1] N. F. Mott, *Metal-Insulator Transition*, Rev. Mod. Phys. **40**, 677-683 (1968).
- [2] M. Imada, A. Fujimori, and Y. Tokura, *Metal-Insulator Transitions*, Rev. Mod. Phys. **70**, 1039 (1998).
- [3] R. Manzke, T. Buslaps, B. Pfalzgraf, M. Skibowski, and O. Anderson, *On the Phase Transitions in 1T-TaS₂*, Europhys. Lett. **8**, 195-200 (1989).
- [4] P. Fazekas and E. Tosatti, *Electrical, Structural and Magnetic Properties of Pure and Doped 1T-TaS₂*, Phil. Mag. B **39**, 229-244 (1979).
- [5] P. Fazekas and E. Tosatti, *Charge Carrier Localization in Pure and Doped 1T-TaS₂*, Phys. B + C **99**, 183-187 (1980).
- [6] P. A. Lee, N. Nagaosa, and X. G. Wen, *Doping a Mott insulator: Physics of High temperature Superconductivity*, Rev. Mod. Phys. **78**, 17-85 (2006).
- [7] J. Schlappa, K. Wohlfeld, K. J. Zhou, M. Mourigal, M. W. Haverkort, V. N. Strocov, L. Hozoi, C. Monney, S. Nishimoto, S. Singh, A. Revcolevschi, J.-S. Caux, L. Patthey, H. M. Rønnow, J. van den Brink, and T. Schmitt, *Spin-Orbital Separation in the Quasi-One-Dimensional Mott Insulator Sr₂CuO₃*, Nature **485**, 82-85 (2012).
- [8] Y. Cao, V. Fatemi, A. Demir, S. Fang, S. L. Tomarken, J. Y. Luo, J. D. Sanchez-Yamagishi, K. Watanabe, T. Taniguchi, E. Kaxiras, R. C. Ashoori, and P. J. Herrero, *Correlated Insulator Behaviour at Half-Filling in Magic-Angle Graphene Superlattices*, Nature **556**, 80-84 (2018).
- [9] C. Dhital, T. Hogan, W. W. Zhou, X. Chen, Z. S. Ren, M. Pokharel, Y. Okada, M. Heine, W. Tian, Z. Yamani,

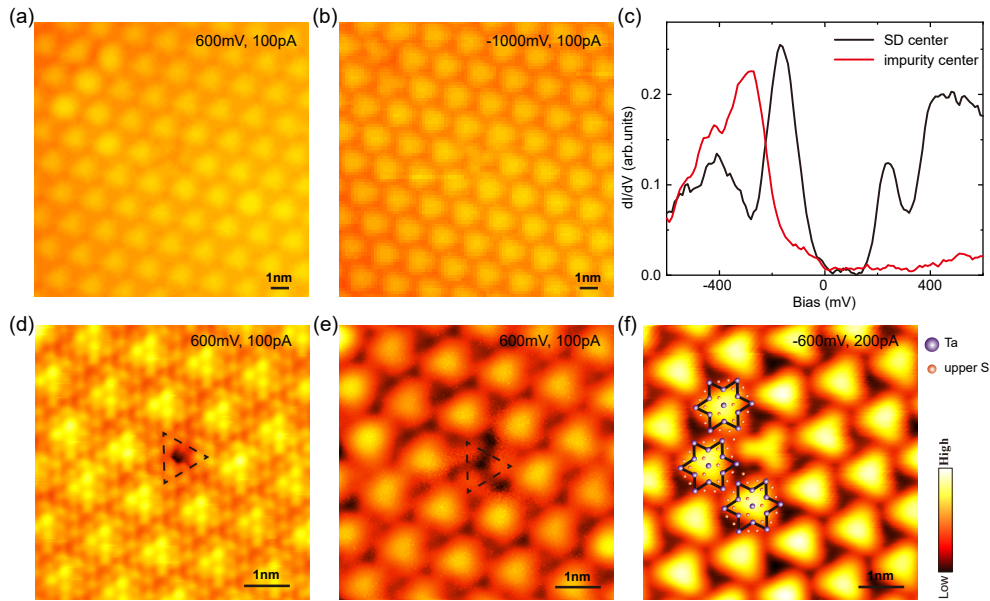


FIG. 6. **Details of the three-petal shaped defect.** (a), (b) Topographies including the same defect under positive and negative bias voltages. The tunneling condition is $V_b = -600$ mV and $I = 100$ pA in (a), and $V_b = -1$ V and $I = 100$ pA in (b). (c) The red and black curves show the dI/dV spectra measured at the center of the three-petal shaped defect and a normal SD. (d) An atomic-resolved three-petal shaped defect under the tunneling condition of $V_b = 600$ mV and $I = 200$ pA. (e) The same defect area in (d). The dashed triangles in (d) and (e) indicate three petals of the defect are at the sites of the three next nearest S atoms. (f) Another topography with a three-petal shaped defect ($V_b = -600$ mV, $I = 200$ pA), with the structure of SD cluster superimposed on the image.

- C. Opeil, J. S. Helton, J. W. Lynn, Z. Q. Wang, V. Madhavan, and S. D. Wilson, *Carrier Localization and Electronic Phase Separation in a Doped Spin-Orbit-Driven Mott Phase in $Sr_3(Ir_{1-x}Ru_x)_2O_7$* , Nat. Commun. **5**, 3377 (2014).
- [10] G. Sclauzero, K. Dymkowski, and C. Ederer, *Tuning the Metal-Insulator Transition in d^1 and d^2 Perovskites by Epitaxial Strain: A First-Principles-Based Study*, Phys. Rev. B **94**, 245109 (2016).
- [11] W. Ch. Lee and A. H. MacDonald, *Modulation Doping Near Mott-Insulator Heterojunctions*, Phys. Rev. B **74**, 075106 (2006).
- [12] B. Sipos, A. F. Kusmartseva, A. Akrap, H. Berger, L. Forró, and E. Tutiš, *From Mott State to Superconductivity in $1T-TaS_2$* , Nat. mater. **7**, 960-965 (2008).
- [13] L. J. Li, W. J. Lu, X. D. Zhu, L. S. Ling, Z. Qu, and Y. P. Sun, *Fe-Doping-Induced Superconductivity in the Charge-Density-Wave System $1T-TaS_2$* , Europhys. Lett. **97**, 67005 (2012).
- [14] Y. Liu, R. Ang, W. J. Lu, W. H. Song, L. J. Li, and Y. P. Sun, *Superconductivity Induced by Se-Doping in Layered Charge-Density-Wave System $1T-TaS_{2-x}Se_x$* , Appl. Phys. Lett. **102**, 192602 (2013).
- [15] J. A. Wilson, F. J. Di Salvo, and S. Mahajan, *Charge-Density-Waves and Superlattices in the Metallic Layered Transition Metal Dichalcogenides*, Adv. Phys. **24**, 117-201 (1975).
- [16] K. L. Bu, W. H. Zhang, Y. Fei, Z. X. Wu, Y. Zheng, J. J. Gao, X. Luo, Y. P. Sun, and Y. Yin, *Possible Strain Induced Mott Gap Collapse in $1T-TaS_2$* , Commun. Phys. **2**, 146 (2019).
- [17] Y. J. Yu, F. Y. Yang, X. F. Lu, Y. J. Yan, Y. H. Cho, L. G. Ma, X. H. Niu, S. Kim, Y. W. Son, D. L. Feng, S. Y. Li, S. W. Cheong, X. H. Chen, and Y. B. Zhang, *Gate-Tunable Phase Transitions in Thin Flakes of $1T-TaS_2$* , Nat. Nanotechnol. **10**, 270-276 (2015).
- [18] A. W. Tsen, R. Hovden, D. Wang, Y. D. Kim, J. Okamoto, K. A. Spoth, Y. Liu, W. J. Lu, Y. P. Sun, J. C. Hone, L. F. Kourkoutis, P. Kim, and A. N. Pasupathy, *Structure and Control of Charge Density Waves in Two-Dimensional $1T-TaS_2$* , Proc. Natl. Acad. Sci. USA **112**, 15054-15059 (2015).
- [19] I. Vaskivskiy, J. Gospodaric, S. Brazovskii, D. Svetin, P. Sutar, E. Goreshnik, I. A. Mihailovic, T. Mertelj, and D. Mihailovic, *Controlling the Metal-to-Insulator Relaxation of the Metastable Hidden Quantum State in $1T-TaS_2$* , Sci. Adv. **1**, e1500168 (2015).
- [20] M. J. Hollander, Y. Liu, W. J. Lu, L. J. Li, Y. P. Sun, J. A. Robinson, and S. Datta, *Electrically Driven Reversible Insulator-Metal Phase Transition in $1T-TaS_2$* , Nano Lett. **15**, 1861-1866 (2015).
- [21] M. Yoshida, R. Suzuki, Y. Zhang, M. Nakano, and Y. Iwasa, *Memristive Phase Switching in Two-Dimensional $1T-TaS_2$ Crystals*, Sci. Adv. **1**, e1500606 (2015).
- [22] I. Vaskivskiy, I. A. Mihailovic, S. Brazovskii, J. Gospodaric, T. Mertelj, D. Svetin, P. Sutar, and D. Mihailovic, *Fast Electronic Resistance Switching Involving Hidden Charge Density Wave States*, Nat. Commun. **7**, 11442 (2016).
- [23] D. Cho, S. Cheon, K. S. Kim, S. H. Lee, Y. H. Cho, S. W. Cheong, and H. W. Yeom, *Nanoscale Manipulation of the Mott Insulating State Coupled to Charge Order in $1T-TaS_2$* , Nat. Commun. **7**, 10453 (2016).
- [24] L. G. Ma, C. Ye, Y. J. Yu, X. F. Lu, X. H. Niu, S. Kim,

- D. L. Feng, D. Tomáánek, Y. W. Son, X. H. Chen, and Y. B. Zhang, *A Metallic Mosaic Phase and the Origin of Mott-Insulating State in 1T-TaS₂*, Nat. Commun. **7**, 10956 (2016).
- [25] S. Qiao, X. T. Li, N. Z. Wang, W. Ruan, C. Ye, P. Cai, Z. Q. Hao, H. Yao, X. H. Chen, J. Wu, Y. Y. Wang, and Z. Liu, *Mottness Collapse in 1T-TaS_{2-x}Se_x Transition-Metal Dichalcogenide: an Interplay Between Localized and Itinerant Orbitals*, Phys. Rev. X **7**, 041054 (2017).
- [26] D. Cho, Y. H. Cho, S. W. Cheong, K. S. Kim, and H. W. Yeom, *Interplay of Electron-Electron and Electron-Phonon Interactions in the Low-Temperature Phase of 1T-TaS₂*, Phys. Rev. B **92**, 085132 (2015).
- [27] D. Cho, G. Gye, J. Lee, S. H. Lee, L. H. Wang, S. W. Cheong, and H. W. Yeom, *Correlated Electronic States at Domain Walls of a Mott-Charge-Density-Wave Insulator 1T-TaS₂*, Nat. Commun. **8**, 392 (2017).
- [28] C. J. Butler, M. Yoshida, T. Hanaguri, and Y. Iwasa, *Mottness Versus Unit-Cell Doubling as the Driver of the Insulating State in 1T-TaS₂*, Nat. Commun. **11**, 2477 (2020).
- [29] H. C. Lin, W. T. Huang, K. Zhao, S. Qiao, Z. Liu, J. Wu, X. Chen, and S. H. Ji, *Scanning Tunneling Spectroscopic Study of Monolayer 1T-TaS₂ and 1T-TaSe₂*, Nano Res. **13**, 133-137 (2020).
- [30] Y. Chen, W. Ruan, M. Wu, S. J. Tang, H. Ryu, H. Z. Tsai, R. Lee, S. Kahn, F. Liou, C. H. Jia, O. R. Albertini, H. Y. Xiong, T. Jia, Z. Liu, J. A. Sobota, A. Y. Liu, J. E. Moore, Z. X. Shen, S. G. Louie, S. K. Mo, and M. F. Crommie, *Strong Correlations and Orbital Texture in Single-Layer 1T-TaSe₂*, Nat. Phys. **16**, 218-224 (2020).
- [31] P. Darancet, A. J. Millis, and C. A. Marianetti, *Three-Dimensional Metallic and Two-Dimensional Insulating Behavior in Octahedral Tantalum Dichalcogenides*, Phys. Rev. B **90**, 045134 (2014).
- [32] M. T. Suzuki and H. Harima, *Electronic Band Structure of 1T-TaS₂ in CDW Phase*, J. Magn. Magn. Mater. **E653**, 272-276 (2004).
- [33] T. Ritschel, H. Berger, and J. Geck, *Stacking-Driven Gap Formation in Layered 1T-TaS₂*, Phys. Rev. B **98**, 195134 (2018).
- [34] S. H. Lee, J. S. Goh, and D. Cho, *Origin of the Insulating Phase and First-Order Metal-Insulator Transition in 1T-TaS₂*, Phys. Rev. Lett. **122**, 106404 (2019).